iScience

CellPress
OPEN ACCESS

Article

The secretory pathway in Tetrahymena is organized for efficient constitutive secretion at ciliary pockets

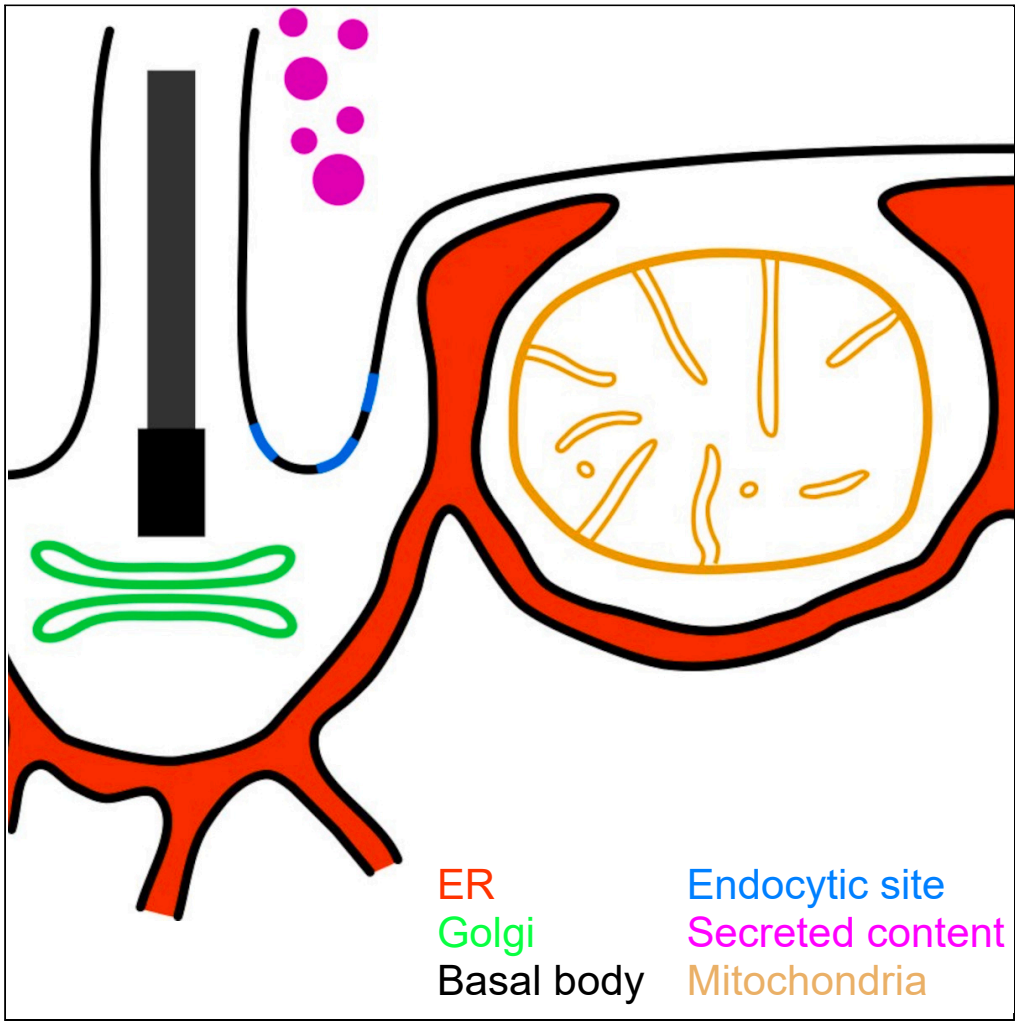

Yu-Yang Jiang, Santosh Kumar, Aaron P. Turkewitz

apturkew@uchicago.edu

Highlights

A fluorescent protein permits live tracing of the secretory pathway in Tetrahymena

Golgi and sites of constitutive secretion are correlated at periodic cortical sites

Golgi exists as stationary and mobile pools, and are concentrated in specific zones

Membrane pockets near basal bodies are dedicated sites of exo/endocytic trafficking

Jiang et al., iScience 27, 111123
November 15, 2024
https://doi.org/10.1016/j.isci.2024.111123

iScience

CellPress
OPEN ACCESS

Article

The secretory pathway in Tetrahymena is organized for efficient constitutive secretion at ciliary pockets

Yu-Yang Jiang,[1,2] Santosh Kumar,[3] and Aaron P. Turkewitz[1,4,*]

SUMMARY

In ciliates, membrane cisternae called alveoli interpose between the plasma membrane and the cytoplasm, posing a barrier to endocytic and exocytic membrane trafficking. One exception to this barrier is plasma membrane invaginations called parasomal sacs, which are adjacent to ciliary basal bodies. By following a fluorescent secretory marker called ESCargo, we imaged secretory compartments and secretion in these cells. A cortical endoplasmic reticulum is organized along cytoskeletal ridges and cradles a cohort of mitochondria. One cohort of Golgi are highly mobile in a subcortical layer, while the remainder appear stably positioned at periodic sites close to basal bodies, except near the cell tip where, interestingly, Golgi are more closely spaced. Strikingly, ESCargo secretion was readily visible at positions aligned with basal bodies and parasomal sacs. Thus peri-ciliary zones in ciliates are organized, like ciliary pockets in the highly unrelated trypanosomids, as unique hubs of exo-endocytic trafficking.

INTRODUCTION

All cells secrete proteins, often prodigiously. For example, it is estimated that 13% of all human genes encode proteins destined for secretion.[1] For a large fraction of proteins secreted in eukaryotes, the process depends on transport through a series of membrane-bounded cytoplasmic organelles, beginning with translocation from the cytoplasm into the endoplasmic reticulum (ER).[2] Delivery of secretory proteins from the ER to the Golgi is then based on the budding and subsequent fusion of vesicles, a mechanism which is repeated for transfer between downstream compartments.[3,4] The final transfer occurs at the plasma membrane where fusion results in extracellular release of the vesicle contents, called exocytosis.[5] Every step in the pathway includes fine-tuning, allowing this conserved eukaryotic pathway to be tailored for cell- and tissue-specific functions. For example, exocytosis itself can be tightly coupled with environmental cues, and this is a key for the activity of many animal tissues.[6] Such *regulated exocytosis*, which relies on the cytoplasmic accumulation of post-Golgi vesicles until their fusion is triggered by extracellular stimuli, can be maintained in cells that simultaneously show *constitutive secretion* of other post-Golgi carriers transporting different cargos.[7] In addition to such temporal control of secretion, cells can spatially direct regulated or constitutive secretion toward specific extracellular targets. In animals and plants, one important mechanism is to position tethering complexes that can capture incoming vesicles, and thereby bias the direction of protein secretion in response to developmental or environmental cues.[8,9] In this manuscript, we investigate the organization of the secretory pathway and the targeting of protein secretion in a protist lineage that is very distantly related from plants or animals.

Ciliates are unicellular organisms that act in many roles ranging from apex microbial predators to parasites, in a wide range of ecosystems.[10] They belong to a wider lineage called Alveolata, whose other members are the apicomplexan parasites and the dinoflagellates.[11] A defining feature of Alveolata are the eponymous alveoli, which are cisternae that underlie the plasma membrane (Figure 1A). Alveoli function in ciliates, at least in part, as reservoirs for mobilizable calcium stores.[12] The alveoli interpose between the cytoplasm and a large fraction of the cell surface, therefore blocking plasma membrane access to structures involved in membrane trafficking,[13–15] including secretory vesicles. Nonetheless, ciliates demonstrate prominent pathways of regulated secretion.[16–21] In *Tetrahymena thermophila*, regulated secretion occurs via 1μM-long secretory granules/lysosome-related organelles called mucocysts, which gain access to the plasma membrane via dedicated docking-and-fusion sites at sutures between adjoining cisternae.[22] Remarkably, the protein assemblies that compose those docking sites appear to be shared with apicomplexans but otherwise not present except within the Alveolata, suggesting that they represent a lineage-restricted secretory adaptation.[23–25]

In contrast, constitutive secretion in ciliates has been documented[26] but the underlying structures and mechanisms are poorly understood. In *T. thermophila*, newly synthesized secretory proteins are secreted to the culture medium within 5 min post-synthesis, suggesting that the

[1]Department of Molecular Genetics and Cell Biology, The University of Chicago, Chicago, IL 60637, USA
[2]AbCellera Boston, Inc. 91 Mystic St, Arlington, MA 02474, USA
[3]National Centre for Cell Science, NCCS Complex, Savitribai Phule Pune University Campus, Ganeshkhind Road, Pune, Maharashtra State 411007, India
[4]Lead contact
*Correspondence: apturkew@uchicago.edu
https://doi.org/10.1016/j.isci.2024.111123

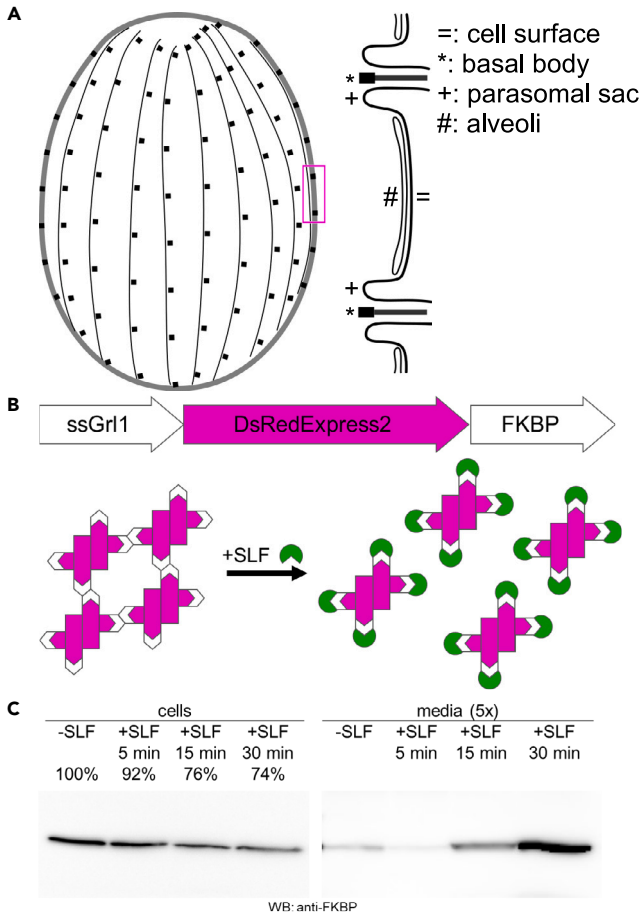

Figure 1. Induced transport of ESCargo in the *Tetrahymena* secretory pathway

(A) Organization of the cell cortex in *Tetrahymena*. A single cell is shown in the cartoon, in which the small black squares represent ciliary basal bodies, which are regularly spaced along cytoskeletal structures called 1° meridians. The boxed zone is expanded on the right, to show two ciliary basal bodies (*) with the adjacent parasomal sacs (+), and alveoli (#) underlying the rest of the surface (=).

(B) The ESCargo variant used in this study consisted of the signal sequence of *T. thermophila GRL1*, linked with tetramerizing dsRed and dimerizing FKBP (top). This protein is designed to enter the endoplasmic reticulum, due to the signal sequence, where it forms aggregates that are trapped, being too large to exit. In the presence of SLF, FKBP dimers dissociate leading to disaggregation, and the protein is free to exit the ER to traverse the secretory pathway.

(C) Western blot of cells and cell-free supernatants, blotted with anti-FKBP antibody. Cell cultures were induced to express ESCargo as described in Materials and Methods. They were exposed to SLF for the times indicated, when aliquots were withdrawn and centrifuged to separate cells from supernatant. Cell supernatants were TCA precipitated, and all samples loaded for SDS-PAGE. The supernatants were loaded at 5-fold higher cell equivalents relative to the cell pellets. The band detected by anti-FKBP western blot is the expected size (38 kD) for the ESCargo polypeptide. For the left-hand panel, the bands were quantified using ImageJ, and the amounts of ESCargo remaining (i.e., non-secreted) in the cells compared to the—SLF sample are indicated.

organization of the ER and Golgi in these cells allows for very rapid transit through the secretory pathway.[27] However, the distributions of these key organelles in *T. thermophila* is not entirely clear, and the prevailing models are largely based on electron microscopy thin sections of chemically fixed samples, many from a somewhat distantly related *Tetrahymena* species, *T. pyriformis*.[13,28] Based on such electron micrographs supplemented by some recent live imaging, the ER extends from just beneath the cortical alveoli too deep in the cytoplasm,[15,28,29] while the Golgi manifest as many small stacks of 1–2 cisternae, historically called dicytosomes, reported to be either distributed throughout the cytoplasm (in *T. pyriformis*) or close to the cell cortex (in *T. thermophila*).[28,30,31] Live cell imaging in *T. thermophila* supported the idea that Golgi are dispersed in a sub-cortical zone over the entire cell surface, forming an array similar to those present for other cortical structures such as ciliary basal bodies.[32,33] Such basal bodies are spaced regularly along cytoskeletal elements called primary meridians, which form ribs spanning the long axis of the cell from peri-apical to the posterior (Figure 1A).[13,33] Mitochondria are also concentrated at the cortex and similarly form an array, though looser than that of the basal bodies, organized along the cytoskeletal meridians.[34,35]

Cortical features of particular interest for this manuscript are plasma membrane invaginations called parasomal sacs, which lie adjacent and anterior to each somatic cilium along the primary meridians (Figure 1A).[13,30,36,37] Analogous structures called ciliary or flagellar pockets in other organisms are implicated in ciliogenesis, cilium-related vesicular trafficking and signaling, and as diffusion barriers between the

plasma and cilia.[38–41] Importantly, parasomal sacs in *Tetrahymena*, together with the mucocyst-docking sites, are the only known zones over much of the cell surface where there is direct contact between the plasma membrane and the cytoplasm.[13] Consistent with this unique accessibility, parasomal sacs are the preferential sites of clathrin-mediated endocytosis in both *Tetrahymena* and *Paramecium*.[42–44] Constitutive secretory cargo may also be released at these sites via exocytosis, but only indirect evidence has thus far been available to address this issue.[28,45]

In the work described in this manuscript we used a recently developed live cell marker to visualize the pathway of constitutive secretion in *Tetrahymena*. Upon synthesis and translocation into the ER, a fluorescent polypeptide called ESCargo accumulates in the form of large aggregates in the ER lumen.[27] The aggregates dissolve upon addition to the cell culture medium of a small molecule, and the now-soluble ESCargo is released for transport into downstream compartments of the secretory pathway. With this reagent and using both wide-field and TIRF microscopy,[46,47] we could visualize compartments of the secretory pathway as well as individual exocytic events. Our live cell data provide an understanding of the functional organization of the ciliate cortex, including secretory compartments as well as mitochondria. Our analysis reveals a key detail underlying the array of cortical Golgi, namely that each Golgi is proximal to a parasomal sac. Moreover, the secretion of ESCargo also occurs at the same cortical positions. Consistent with the idea that zones of active secretion are spatially delimited, successive exocytic bursts occur at the same positions. Our results argue that the parasomal sacs are hubs of both endocytic and exocytic trafficking, and they provide a newly detailed and global mapping of cortical organization in a ciliate.

RESULTS

Small molecule-induced dispersal of ESCargo leads to its rapid secretion from *T. thermophila*

In order to investigate the pathway of constitutive secretion in *Tetrahymena*, we took advantage of the artificial fluorescent secretory protein Erv29/Surf4-dependent secretory cargo (ESCargo), expressing it under the control of the cadmium-inducible *MTT1* promoter (Figure 1B).[48] We previously showed that ESCargo, initially developed in yeast, could be modified with a *Tetrahymena*-derived signal sequence to act as a secretory protein in *T. thermophila*.[27,49,50] The logic underlying the design of ESCargo is shown in Figure 1B, with the key point being that addition of the small molecule SLF (synthetic ligand of FKBP) dissociates ESCargo aggregates that form in the ER, allowing the now-soluble proteins to exit and advance through the secretory pathway.

The N-terminal signal sequence in our current construct is slightly modified from that used in the previous study (see STAR★Methods).[27] To confirm ESCargo secretion for the new construct, we exposed cells to SLF and subsequently measured the amount of ESCargo released into the culture supernatant. A significant amount of secreted ESCargo was detectable within 15 min of SLF exposure, while cell-associated ESCargo decreased by ~25% in the same period. This is on par with results using the prior construct,[27] and it encouraged us to ask whether the secreted pool could be visualized by microscopy. We note that a significant portion of ESCargo remained in the cell after 30 min (Figure 1C).

The cortical endoplasmic reticulum, traced using SLF-dispersed ESCargo and GFP-KDEL, cradles an array of mitochondria

We exposed cells expressing ESCargo to SLF for 5–15 min and immobilized them in CyGel (ab109204, Abcam; STAR★Methods) for fluorescence microscopy. Live cell imaging revealed fluorescence throughout the cell (Figures 2A and 2B). Just beneath the cell surface, elongated fluorescent structures appeared to be organized along the regularly spaced meridians, branching to create an irregular reticulum (Figures 2A, S1A, and S1B). Deeper in the cytoplasm, ESCargo fluorescence surrounded the nuclei as well as appearing to partially or completely encircle other heterogeneous circular structures (Figure 2B). This pattern appeared consistent with the expectation that SLF-dispersed ESCargo primarily occupies the ER lumen. To visualize the ER lumen directly, we expressed GFP bearing an N-terminal signal sequence and a C-terminal "KDEL" motif, reported previously to serve as an ER marker in *Tetrahymena*[51] as it does in many other eukaryotes. The localization of ss-GFP-KDEL appeared markedly similar to that of ESCargo, including distinct patterns at the cortical vs. deeper cytoplasm. (Figures 2C, 2D, and S1E–S1H). At the cortex, the ss-GFP-KDEL signal often appeared in the form of loops whose openings faced the plasma membrane (Figure 2D, inset). The regularity of the loop dimensions suggested that pockets of cortical ER might be cradling a single class of structures. Deeper in the cytosol, open or closed loops appeared to be associated with heterogeneous compartments. In our live cell imaging the overall distribution of ss-GFP-KDEL-labeled structures appeared relatively static, except for motion close to the pulsatile contractile vacuole.[52]

We confirmed that ESCargo and ss-GFP-KDEL were labeling the same structures by co-expressing them. In these cells, ss-GFP-KDEL was constitutively expressed while ESCargo expression was induced by exposure to cadmium. In SLF-free medium, ESCargo in induced cultures appeared as large and bright puncta within the dispersed ER reticulum marked by ss-GFP-KDEL (Figure 2E and 2F). These puncta correspond to the expected ESCargo aggregates within the ER lumen. Following exposure to SLF, the ESCargo puncta disappeared and were replaced by the dispersed signal shown above. This dispersal was rapid, complete in the time needed to prepare a microscope slide, which prevented us from determining its precise time course. We imaged the ESCargo as well as ss-GFP-KDEL cortical distributions in these cells using TIRF microscopy, and found striking overlap as expected (Figures 2G, S1L, and S1J).

TIRF microscopy also allowed additional examination of the striking cortical distribution of the ER, which was apparent by either ESCargo or ss-GFP-KDEL fluorescence. In particular, patches of ER surrounded numerous elliptical spaces, relatively homogeneous in size that formed an array between meridians. This pattern of ellipses was reminiscent of the known distribution of cortical mitochondria in *Tetrahymena*.[34] To visualize the mitochondrial distribution in live cells, we used MitoTracker Green to stain cells expressing a marker for primary meridians, the basal body protein Poc1p-mCherry.[53] Consistent with previous reports, mitochondria were distributed over the cell cortex except along the narrow primary meridians marked by rows of basal bodies (Figure S2). We then visualized the fluorescent green mitochondria in cells also

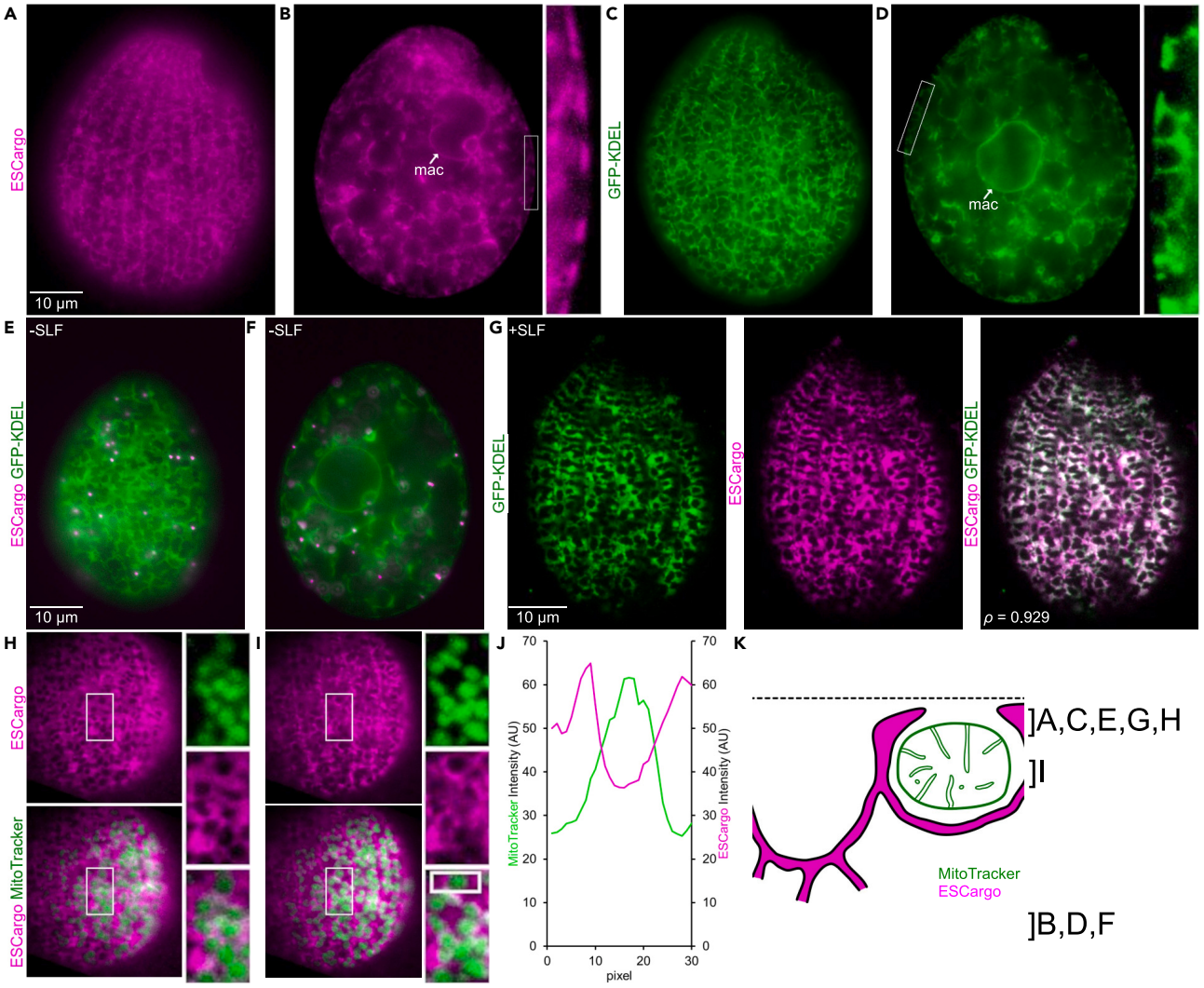

Figure 2. Live imaging of cells expressing ESCargo and GFP-KDEL

(A and B) A cell expressing ESCargo after exposure to SLF. (A) Near the cell surface, a fluorescent reticulum features regularly spaced ridges extending the length of the cell. (B) In a cell mid-section, the fluorescent reticulum appears to surround heterogeneous cytoplasmic organelles including the macronucleus (mac). The boxed area, expanded in the right hand panel, highlights the punctuated ESCargo fluorescence at the cell periphery.

(C and D) A cell expressing GFP-KDEL. (C) Near the cell surface, the pattern of fluorescence as in (A) appears as a reticulum with ridges. (D) In a cell midsection, the fluorescent ER appears as in B to surround heterogeneous structures including the Macronucleus (mac). At the very edge of the cell, the fluorescent ER appears to loop around structures in a way that leaves openings toward the cell exterior, as shown in the expanded inset. Overall, the ER organization revealed by ESCargo and GFP-KDEL are very similar. See also Figure S1.

(E and F) A cell expressing ESCargo and GFP-KDEL but without addition of SLF. Large and bright ESCargo puncta are present in the GFP-KDEL-labeled ER reticulum both near the cortex (E) and deep in the cytoplasm (F).

(G) A cell expressing ESCargo and GFP-KDEL after exposure to SLF, imaged using TIRF microscopy (TIRFM). The GFP-KDEL pattern (left panel) is closely mirrored by the dispersed ESCargo pattern (middle panel), with the overlap shown in the right panel indicated by the pale gray areas. The Pearson coefficient (ρ) is 0.929. Similar imaging and analysis of a second cell in S1I and S1J resulted in Pearson coefficients of 0.921 and 0.875, respectively.

(H and I) A cell containing SLF-dispersed ESCargo, incubated with MitoTracker Green, and imaged using TIRFM. (H) In the thin optical section captured with TIRFM, the cortical ER labeled with ESCargo has many gaps, many of which appear circular. Those gaps in ER labeling stain green with MitoTracker, as shown most clearly in the expanded inserts. The MitoTracker-stained mitochondria appeared at a focal level close to that in (G). (I) The same cell shown in H, but imaged at a slightly deeper focal plane. The mitochondria are most clearly focused in this plane (compare inserts in H and I).

(J) Intensity plots of ESCargo and MitoTracker Green along the length of the rectangle outlined in panel I, bottom right. The mitochondrion appears to be circumscribed by ER, with very limited overlap.

(K) A cartoon of the edge of a cell midsection, illustrating the putative organization of the ER, indicated by ESCargo, and mitochondria near the cell cortex. Focal planes corresponding to panels A–I are indicated. Dashed line indicates an imaginary plane parallel to the coverslip.

expressing ESCargo, under conditions in which the latter was dispersed in the ER. Analysis of these cells by TIRF microscopy confirmed that cortical mitochondria are enclosed by the cortical ER reticulum, i.e., mitochondria largely or entirely constitute the array of ellipses noted previously (Figures 2H–2J). We combined this TIRF perspective with the images showing that ER also traces the elliptical spaces at their proximal sides (Figures 2B and 2D, insets). Based on these images, we infer that the ER cradles the mitochondria on all sides except that facing the plasma membrane. Additionally, in some side views the ends of ER near the plasma membrane appear to widen and thereby closely follow the contour of the mitochondria (Figures 2B and 2D, insets), an interpretation also consistent with the top views (Figure 2G). The images also indicate the likelihood that the ridges of subcortical ER align with primary meridians (compare Figures 2H and 2I with Figure S2). The model resulting from these results is shown in Figure 2K.

In other organisms, tether-dependent close contacts between the ER and mitochondria are important for lipid transfer as well as calcium regulation.[54] Lipid transfer in yeast depends on a heterotetrameric complex called ERMES.[55] Interestingly, we could identify homologs for two of the ERMES subunits in *Tetrahymena*, including the gem1 subunit (TTHERM_00502190). The second relevant Tetrahymena protein (TTHERM_00485870), has an N-terminal domain, as part of a larger protein, with predicted structural similarity to both mmm1 and mdm12, the ERMES subunits that are directly involved in lipid transfer.[56]

The dispersal of ESCargo throughout the ER lumen in response to SLF was reversible. That is, when cells were immobilized in CyGel not containing SLF, the dispersed ESCargo was rapidly replaced by numerous small puncta (Video S1). The reaggregation of ESCargo in the absence of an extracellular pool of SLF could be eliminated by including SLF in the CyGel buffer. When cells were immobilized in such SLF-oversaturated CyGel, dispersed ESCargo persisted in ER lumen for over 30 min. This agrees with the result in Figure 1C, that large amounts of ESCargo persist in the cell even after exposure to SLF. Prolonged exposure to SLF sometimes led to additional faint ESCargo accumulation in cortical spots along the primary meridians, and these did not overlap with the cortical ER (Figure S3). These spots hint at post-ER compartments that could represent intermediates in secretory protein transport from the ER to the plasma membrane.

Cortical Golgi, visualized by live cell imaging of Rab6C and Gef1p, are located close to ciliary basal bodies along 1° meridians

Based on well-established models for eukaryotic membrane trafficking, and also consistent with the patterns of glycosylation of *Tetrahymena* secretory proteins (see Weide et al.[57] and refs therein), ESCargo trafficking from the ER to plasma membrane is expected to involve transport through the Golgi dictyosomes. Electron microscopic studies of *T. pyriformis* revealed that individual dictyosomes often were positioned adjacent to cortical mitochondria, but did not reveal their global distribution (see Figure S2 for cortical mitochondria organization).[28] In live *T. thermophila*, this distribution was analyzed by imaging of Rab6, a conserved Golgi-associated protein. GFP-tagged Rab6 appeared as an array of cortical puncta that were aligned along rows, but their position relative to established cortical landmarks was not determined.[32]

To better understand where the Golgi were positioned in these cells, we co-expressed GFP-Rab6Cp together with Poc1p-mCherry as a marker for 1° meridians. Strikingly, most GFP-Rab6Cp puncta were closely adjacent to those of Poc1p-mCherry, suggesting that dictyosomes were specifically positioned near basal bodies (Figure 3A). To bolster this result, we established another Golgi marker for live cell microscopy. *T. thermophila* TTHERM_00569500 is homologous to the Sec7 domain-containing ADP-Ribosylation factor guanine nucleotide exchange factor 1 (GEF1) and to BIG1, which are Golgi-associated proteins in other organisms.[58,59] Like for Rab6Cp, imaging of *Tetrahymena* Gef1p-GFP revealed puncta positioned near Poc1p-mCherry along the 1° meridians (Figure 3B).

Interestingly, the patterns of both GFP-Rab6Cp and Gef1p-GFP also included series of closely spaced puncta that filled the interval between two or more basal bodies. These closely spaced series occurred exclusively at the cell apex, where the basal bodies are also more closely spaced, and were even more prominent in dividing cells at the zone immediately posterior to the division plane (Figure S4).

Some Golgi are strikingly mobile, and this population is enriched in a subcortical zone

Because the fluorescent signals of GFP-Rab6Cp, and of Gef1p-GFP in particular, were close to the background of cytosolic autofluorescence, visible particularly as large spherical food vacuoles, it was difficult to judge whether the proteins were also associated with structures deeper in the cell. To improve signal intensity, we endogenously tagged *GEF1* with mNeon.[60] Live imaging of cells expressing Gef1p-mNeon, compared to the GFP-tagged version, showed similar but more defined cortical arrays along the 1° meridians (Figure 3C). The number of GEF1p-mNeon spots sharply decreased when the plane of focus was adjusted deeper into the cytoplasm (Figure 3D), consistent with the idea that the dictyosomes are primarily distributed in the cortical zone of the cell.

In our live cell imaging, the Golgi at the cortex appeared largely stationary. In contrast, strikingly mobile GFP-Rab6Cp- or Gef1p-mNeon-labeled Golgi were encountered in the subcortical zone, which we defined as the slightly deeper plane in which basal bodies and cortical mitochondria were largely absent (Videos S2 and S3). These Golgi moved rapidly and directionally over long distances. The mobile Golgi appeared largely restricted to that subcortical plane, being comparatively rare both at the cortex and deeper in the cytoplasm.

ESCargo in SLF-induced cells can be visualized in mobile Golgi

Cells expressing ESCargo maintain bright fluorescence in the ER after SLF dispersal, as shown previously. This persistent bright background made it difficult to analyze ESCargo in the stationary cortical Golgi, which are in a focal plane close to that of the ER. We, therefore exploited the motile Golgi population easily visible in most cells, at a focal plane deeper in the cytoplasm, to confirm that ESCargo traverses this organelle. First, using TIRF imaging of cells containing dispersed ESCargo, we detected rapid and directional movements of compartments containing ESCargo at the sub-cortical focal plane, as expected if ESCargo were present in mobile Golgi (Video S4). To validate this

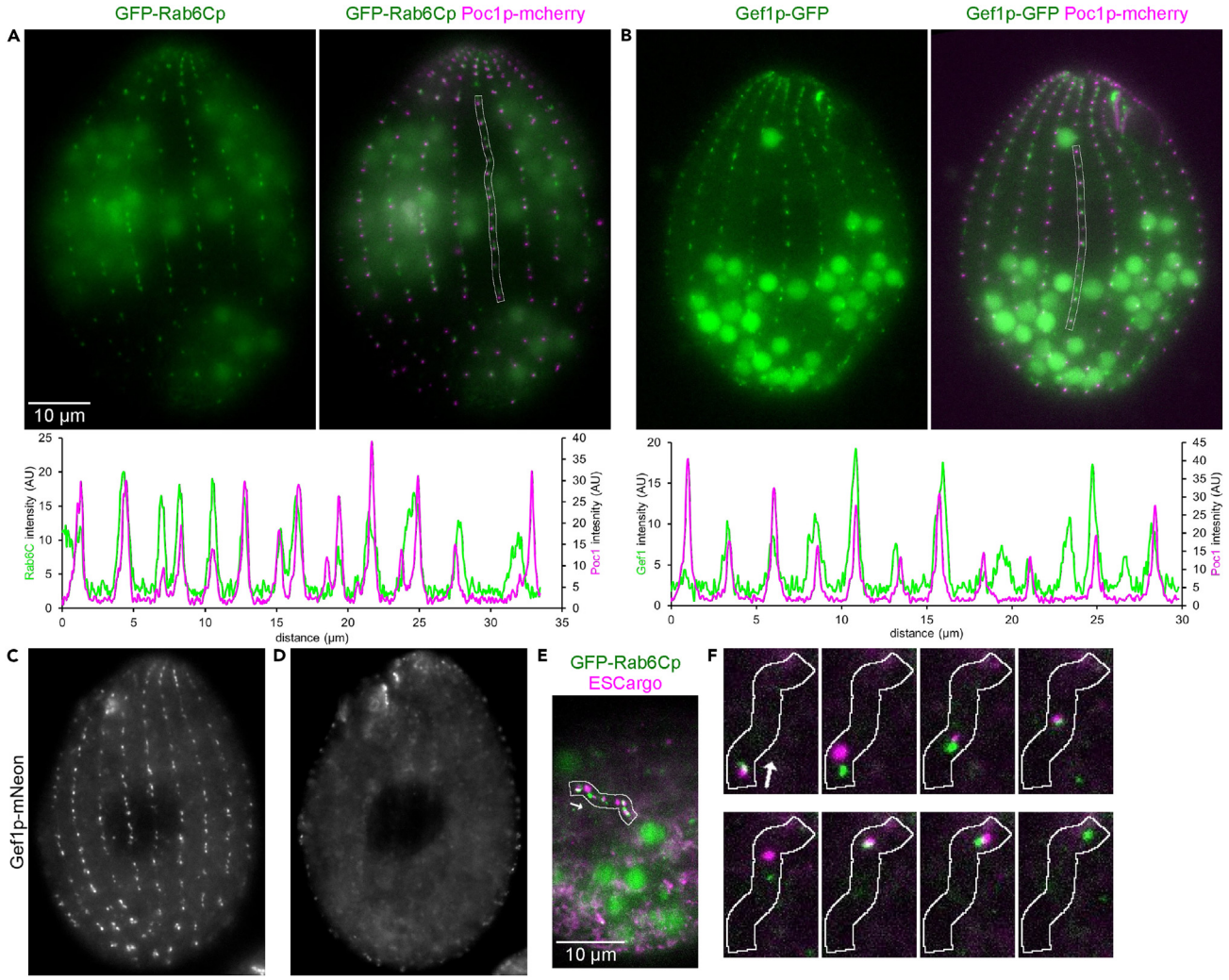

Figure 3. Live imaging of Golgi, ciliary basal bodies, and ESCargo

(A) A cell expressing GFP-Rab6Cp and Poc1p-mCherry. Cortical GFP-Rab6Cp (green) localizes adjacent to Poc1p-mCherry (magenta) along the length of the 1° meridians. In the bottom panel, the intensities of the two signals are plotted from top to bottom along the highlighted region, underscoring their near-colocalization within the array. GFP-Rab6Cp is also seen on mobile compartments in the subcortical region (Video S2).

(B) A cell expressing Gef1p-GFP and Poc1p-mCherry. Cortical Gef1p-GFP localization is similar to that of GFP-Rab6Cp, but its relatively weaker fluorescence intensity resulted in higher background signals.

(C and D) A cell expressing Gef1p-mNeon. (C) As expected for a Golgi-associated protein, Gef1p-mNeon signal is prominently associated with an array of immobile structures near the cortex. (D) Few distinct Gef1p-mNeon labeled structures are found deeper in the cytoplasm. Gef1p-mNeon is also seen on mobile compartments in the subcortical region (Video S3).

(E) A projected image from a time series of a cell expressing GFP-Rab6Cp and ESCargo. The path of a moving compartment containing ESCargo and GFP-Rab6Cp was highlighted. Because the two colors are captured sequentially rather than simultaneously, they mark slightly different positions for the moving compartment. See also Figure S5.

(F) Frames of the highlighted movement from the time series shown in (E).

interpretation, we analyzed cells expressing both ESCargo and GFP-Rab6C. Notably, ESCargo was visible in a subset of the subcortical GFP-Rab6Cp-positive mobile compartments (Figure 3E and 3F and S5). These observations support the idea that ESCargo upon exit from the ER is transported through the classical secretory pathway via the Golgi. Consistent with this view, ESCargo also localized to stationary meridional structures likely to be cortical dictyosomes (compare Figure S3 to Figures 3A–3C).

ESCargo secretion is visible by TIRF microscopy

The positioning of Golgi near to basal bodies suggested that post-Golgi carriers might efficiently fuse with and release their secretory cargo at the adjacent parasomal sacs. To detect ESCargo release from cells we again took advantage of TIRF microscopy. We modified our general

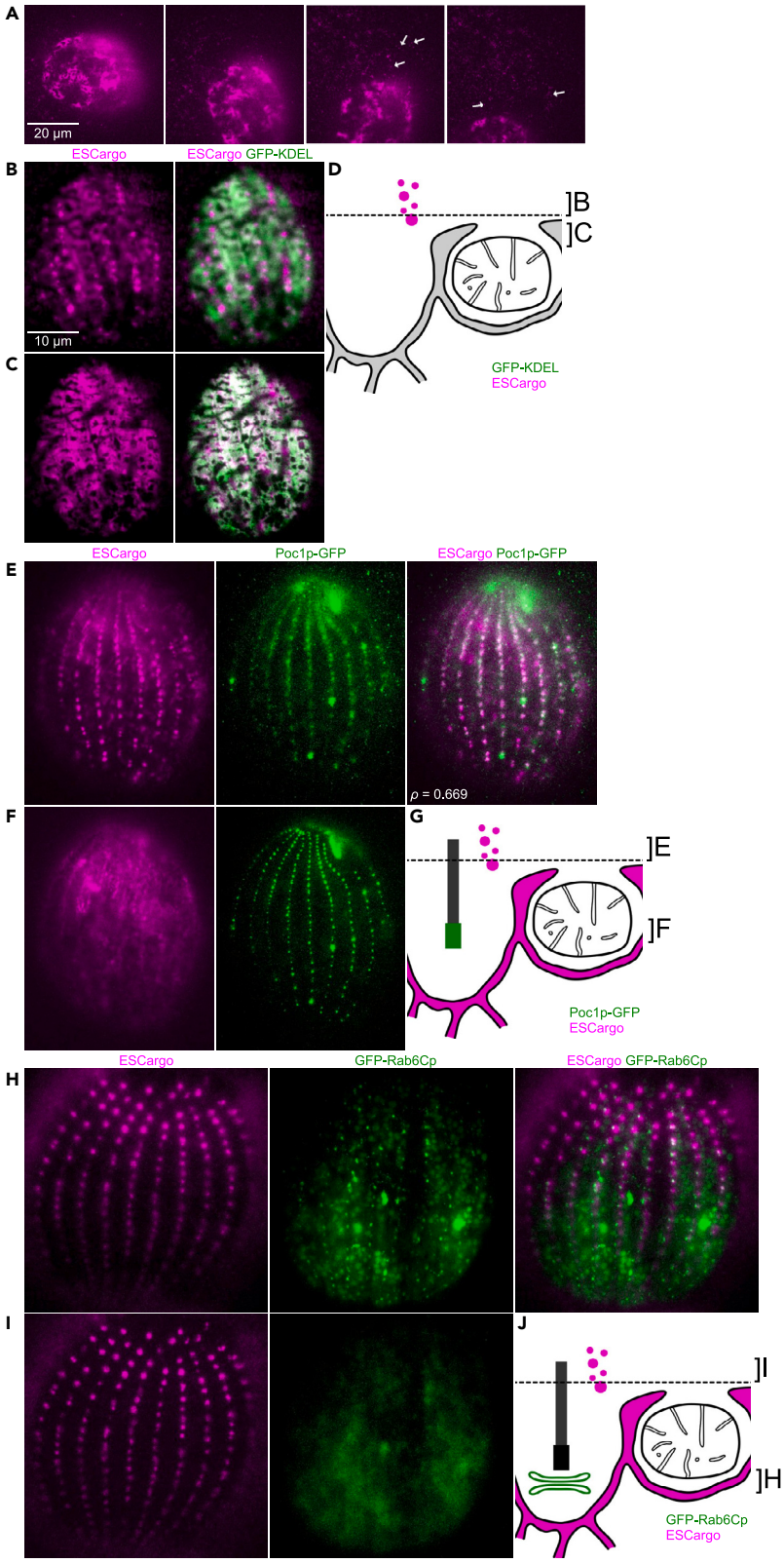
A
20 μm
ESCargo
ESCargo GFP-KDEL
B
10 μm
C
D
]B
]C
GFP-KDEL
ESCargo
ESCargo
Poc1p-GFP
ESCargo Poc1p-GFP
E
ρ = 0.669
F
G
]E
]F
Poc1p-GFP
ESCargo
ESCargo
GFP-Rab6Cp
ESCargo GFP-Rab6Cp
H
I
J
]I
]H
GFP-Rab6Cp
ESCargo

Figure 4. Live imaging of ESCargo secretion

(A) Select frames from a TIRF recording of a cell expressing ESCargo. Deposits of ESCargo are visible as speckles (arrows) in the area behind the advancing cell. Full recording in Video S5.

(B and C) TIRF imaging of a cell expressing ESCargo and GFP-KDEL. The cell was rapidly immobilized by being firmly pressed against the coverslip, while being exposed to SLF. (B) ESCargo deposits between the cell surface and the cover glass are detected at discrete sites. (C) At a lower focal plane, similar to that in Figure 2G, both ESCargo and GFP-KDEL are seen to fill the ER. Full recording in Video S6.

(D) A cartoon of secreted ESCargo and subcortical ER with luminal ESCargo and GFP-KDEL, indicated by the pale gray area. Focal planes corresponding to panels (B) and (C) are indicated.

(E and F) TIRF imaging of a cell expressing ESCargo and Poc1p-GFP. (E) (left panel) Secreted ESCargo deposits are visible extracellularly, as in (B). At this focal plane, Poc1p-GFP is poorly focused (middle panel). (F) At a lower focal plane, ESCargo is poorly focused while in-focus cortical Poc1p-GFP defines the basal body distribution along the 1° meridians. The merged image in E (third panel) shows the ESCargo deposits align with the 1° meridians, and in many cases are in close proximity to basal bodies. The Pearson coefficient (ρ) is 0.669.

(G) A cartoon of secreted and ER luminal ESCargo, and Poc1p-GFP at the basal body. Focal planes corresponding to panels (E) and (F) are indicated.

(H and I) TIRF imaging of a cell expressing ESCargo and GFP-Rab6Cp. (H) The focal plane was chosen to image cortical GFP-Rab6Cp-labeled Golgi. (I) The focal plane was chosen to image extracellular ESCargo deposits. The merged image in H (third panel) shows the ESCargo deposits align closely to the stationary Golgi along 1° meridians. Similar TIRF imaging of another sample is shown in Figure S6.

(J) A cartoon of ER and secreted ESCargo with most Rab6Cp-labeled Golgi localized near basal bodies. The precise positioning of the Golgi relative to the basal bodies is not established. Focal planes corresponding to panels (H) and (I) are indicated.

TIRF protocol, using smaller volumes of cells and SLF-saturated CyGel, to optimize cell immobilization and to potentially slow the diffusion of soluble tetrameric ESCargo following its release from the cell surface. By first focusing on cells that were poorly immobilized, we noted that secreted ESCargo deposits were readily detectible, appearing after a short lag in the wake of the swimming cell (Figure 4A; Video S5). These deposits remained as bright puncta for short periods after being released, and may represent transient ESCargo aggregates. Similar deposits were visible in immobilized cells at a focal plane superficial to the cortical ER (Figures 4B–4D; Video S6), likely between the plasma membrane and the coverslip. Bursts of ESCargo seen repeated at fixed positions (Video S6) were likely to represent successive individual exocytic events occurring at the same plasma membrane zone. Altogether, these observations appear to suggest that ESCargo is released at discrete locations regularly spaced along meridians.

ESCargo secretion occurs at discrete sites that align with stationary Golgi and with ciliary basal bodies

To ask whether the positions of the secreted ESCargo deposits aligned with basal bodies and their adjoining parasomal sacs, we analyzed ESCargo secretion from cells expressing Poc1p-GFP. We compared the positions of ESCargo deposits, in an extracellular focal plane, with the positions of Poc1p-GFP in a cortical focal plane. The alignment of the signals in the two focal planes provided strong evidence that the secretion sites were at or near the basal bodies along the 1° meridians (Figures 4E–4G). As expected given this alignment, the positions of the ESCargo deposits in many cases correlated with those of the GFP-Rab6Cp-labeled cortical Golgi (Figures 4H–4J and S6).

In *Trypanosomes*, a GPI-linked protein appears to depend on the contractile vacuole, an organelle that undergoes periodic fusion with the plasma membrane, for delivery to the cell surface.[61] We never detected ESCargo localized to the contractile vacuole in *Tetrahymena*, nor any bursts of ESCargo release coincident with contractile vacuole emptying.

Parasomal sacs, with associated Golgi, are dedicated hubs of endocytic and exocytic trafficking

Based on the evidence presented previously, constitutive secretion occurs along 1° meridians and very close to ciliary basal bodies. Importantly, neither epifluorescence nor TIRF microscopy revealed ciliary ESCargo fluorescence in any experiment. This argues strongly against the possibility that the ciliary membrane and/or ciliary tip represent secretion sites for ESCargo. Instead, our data provide strong support for the long-standing hypothesis that constitutive secretion occurs from the parasomal sacs, one of the few zones in these cells where the plasma membrane is accessible to the cytoplasm without an intervening layer of alveoli. Our data therefore argue strongly for a model in which parasomal sacs, with closely neighboring Golgi, are dedicated zones for both endocytic and exocytic membrane traffic in *Tetrahymena* (Figure 5).

DISCUSSION

The transport of newly synthesized secretory proteins through a discrete set of endomembrane compartments, ending in their release via exocytic membrane fusion, was largely defined by studies in mammalian cells and subsequently in budding yeast.[62,63] Understanding the generalizability of the resulting models beyond the Opisthokont lineage, to which both animals and yeast belong, depends on research in other lineages.[64] For example, research on the secretory pathway in land plants (Archaeplastida/Viridiplantae) has demonstrated that the broad pathway outline is shared with Opisthokonts, but has also revealed remarkable lineage-specific adaptations at both the compartmental and molecular levels.[65–67]

In the Alveolata lineage of protists, which includes ciliates and apicomplexans, a well-studied secretory pathway based on lysosome-related organelles evolved unique and lineage-restricted machinery to control the locus and timing of exocytosis.[23,68–70] The classical secretory pathway in these organisms, in contrast, has received scant attention. One major finding of this paper is to locate the sites of constitutive protein secretion in a ciliate. Constitutive secretion of endogenous proteins has been detected biochemically in *Tetrahymena*.[26,71] Since the kinetics of ESCargo release from the cell are similar to those of endogenous proteins measured by biosynthetic pulse-chase analysis,[71]

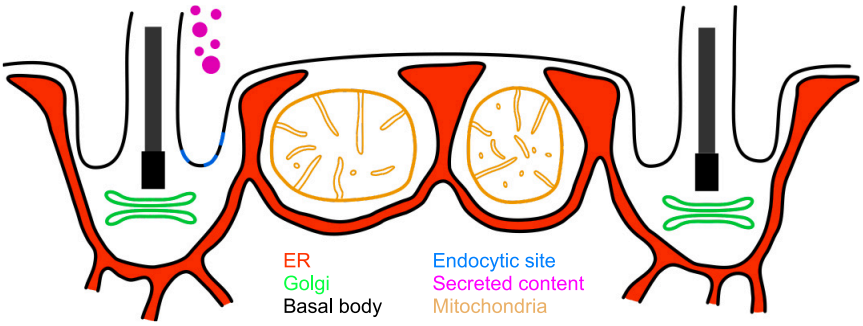

Figure 5. A cartoon illustrating the architecture of the T. thermophila secretory pathway in the context of other cortical features explored in this study
Prior results on endocytosis at the parasomal sacs are included.[43,44] For simplicity, the alveoli are not included.

ESCargo is likely to accurately reflect a pathway traversed by native proteins. The only sequences in our ESCargo construct belonging to a secretory protein are the N-terminal 18 amino acids, derived from *T. thermophila* Grl1p, and these are expected to be cleaved after the protein enters the ER.[72] The ESCargo polypeptide is therefore likely to travel with bulk flow through the secretory pathway,[73] though we cannot exclude the possibility that it contains an adventitious sorting motif for *Tetrahymena*. In the ESCargo construct originally engineered for *S. cerevisiae*, the fluorescent protein moved rapidly from the ER to the Golgi shortly after its induced disaggregation, due to an ER exit motif within the construct.[27] Whether ciliate secretory proteins possess ER exit motifs remains to be determined, but if so they are unrecognizable based on sequence similarity to those in yeast and animals. The construct we used in the current paper lacks a functional exit motif, which can explain why a large fraction of the disaggregated ESCargo persists in the ER.

Our data argue strongly that small plasma membrane invaginations called parasomal sacs are the major, and likely unique, sites where constitutive secretion occurs in *T. thermophila*. Since parasomal sacs are also the dedicated sites of clathrin-mediated endocytosis in *Tetrahymena*,[43] they represent trafficking hubs at the cell surface. In the apicomplexan and dinoflagellate branches of Alveolates, structures called micropores are invaginations between alveolar cisternae, and have recently been shown in the apicomplexan *Toxoplasma gondii* to be sites of endocytosis; whether they are also sites of secretion has not yet been investigated.[14] The similarities between parasomal sacs in ciliates and micropores in apicomplexans raise the question of whether they represent homologous structures.

Interestingly, in *Tetrahymena* each basal body/parasomal sac-centered cortical unit constitutes a domain whose response to cytoplasmic morphogens, repeated over the cell surface, governs cellular patterning through the cell cycle.[74–79] More broadly, these cortical units can be conceived of as self-sustaining, self-replicating, and self-propagating.[80] In that context, it is intriguing that the findings in our current study suggest that many aspects of membrane trafficking within each cortical unit could be substantially autonomous.

At the parasomal sacs, homeostatic linkage between outward and inward membrane trafficking may be required in part to maintain the membrane surface, analogous to the exocytic-endocytic coupling associated with animal cell neurotransmission,[81] or more recently studied in plants.[82] To explore this idea in ciliates, it would be interesting to ask whether disrupting constitutive secretion, for example with a small molecular inhibitor, quickly downregulates endocytosis at parasomal sacs. Unfortunately the tools to pursue such experiments are not yet well developed in *Tetrahymena*. Brefeldin A (BFA) can be used to block ER-to-Golgi traffic in many organisms, but in multiple trials over a wide range of concentrations we found that BFA has no significant effect on localization of Golgi markers or ESCargo secretion. Another interesting question is whether mechanisms to maintain membrane surface in *Tetrahymena* include cross-talk with other pathways that involve membrane addition or retrieval at the plasma membrane, such as exocytosis of lysosome-related organelles, or the formation of phagosomes and their eventual fusion with the plasma membrane to expel undigested contents.[83] Interestingly in ciliates, these specialized pathways occur at distinct and non-overlapping plasma membrane domains and could potentially rely on pathway-internal homeostatic mechanisms; for example, rapid vesicle endocytosis at the sites of phagosome exocytosis may directly provide the membrane for phagosome formation, even though this occurs at the far end of the cell, tens of microns distant.[32,84]

The organization of membrane trafficking near cilia we describe is not unique to *Tetrahymena*. In mammalian cells, there is some evidence that periciliary invaginations which resemble parasomal sacs may constitute preferential secretory sites, while in Trypanosomes a pocket flanking the sole cilium has been clearly established as the cellular hub for endo/exocytosis.[38–41] One prominent feature of this ciliary pocket in Trypanosomes is an adjacent Golgi. Strikingly, we found a similar arrangement in *Tetrahymena*: most Golgi are present at the cortex and are closely adjacent to ciliary basal bodies and therefore to parasomal sacs. These live cell observations are compatible with results from some prior EM-based studies, which placed Golgi adjacent to cortical mitochondria or near the base of cilia.[28,30,31] We also detected a 2nd population of mobile Golgi somewhat deeper in the cytoplasm, and these were strikingly mobile while those at the cortex appeared relatively stationary. ESCargo was found associated with both populations, but the mobile Golgi could potentially provide distinct functions, not only processing but also distributing secretory products, as suggested by recent studies in *Arabidopsis*.[85–87] We do not yet know the distribution of ER exit sites (ERES) in Tetrahymena, which would be informative for interpreting the mobile Golgi. Mobile Golgi could be detected in our previous study in Tetrahymena, but they were neither discussed nor recognized as inhabiting a different cellular plane from the stationary population.[32] In a later study, mobile structures were detected but not identified as Golgi.[31]

The ciliates and trypanosomids belong to two different eukaryotic supergroups, the former as alveolates within the SAR supergroup, and the latter as Euglenozoa in the Discoba supergroup.[88] Thus, the similarities in the organization of periciliary invaginations as sites of endo/exocytosis, and moreover associated with adjacent Golgi, could hint at an ancestral eukaryotic feature, potentially present in the last eukaryotic common ancestor (LECA).[89] To test this hypothesis, the key question is whether the similar organization in the two lineages results from homologous determinants. The alternative is that the similar organization results from independent innovations in the two lineages, and therefore reflects convergent evolution. Since some of the determinants have already been uncovered in trypanosomids,[90,91] an important aim is to accomplish the same in ciliates.

Our live cell Golgi imaging relied on endogenous N-terminal tagging of *RAB6C*, one of four *RAB6* genes in *T. thermophila*.[32] Whether Rab6Cp associates with a Golgi subcompartment is not known, but the four Rab6 paralogs show highly similar localization patterns.[32] To test our conclusions using another compartmental marker, we endogenously tagged *GEF1*, whose homologs in other organisms are Golgi-associated.[58] Gef1p was previously described as a ciliary protein in *Tetrahymena*, but it was never directly localized in those studies.[92] In imaging the endogenously tagged Gef1p, we never detected ciliary localization but instead observed localization consistent with Golgi targeting, indistinguishable from that of Rab6Cp.

Tetrahymena are dramatically polarized for phagocytosis, with phagosomes formed at the anterior oral apparatus, while undigested phagosome contents are excreted at a posterior cytoproct. Similarly, some Rab GTPases associated with early and recycling endosomes show a polarized distribution.[32] More evidence for polarized trafficking comes from experiments following the uptake of a bulk endocytic marker, where endocytosis occurred at parasomal sacs over the entire cell surface but the marker was subsequently transported within minutes to a tubulovesicular compartment near the cell posterior.[43] In this paper, we find that secretion may also be polarized: the Golgi are present over the entire cell cortex but with higher density at the anterior end of the cell and, in dividing cells, just posterior to the division plane in what will form the anterior end of one daughter. In these regions, multiple closely spaced Golgi are present, still associated with 1° meridians but many not adjacent to the basal bodies. These zones of concentrated Golgi may represent zones of more active or potentially specialized secretion.

The zone-specific enrichment of Golgi is particularly suggestive in the context of anterior-posterior cortical patterning that is a striking feature of ciliates. As pointed out in the study by Cole et al.,[80] cortically delimited kinases could be determinants of localized remodeling, inducing the formation of polarized zones or gradients that shape cellular pattern formation. Interestingly, in the species *Tetrahymena pyriformis*, immunolocalization data with cross-specific antibodies suggest that the cells have zones enriched in cell cycle-specific phosphoproteins[93]; remarkably, those zones are indistinguishable in position from those where we detect a high density of Golgi in *T. thermophila*. One model for thinking about these connections comes from the small GTPase Cdc42, which in several classical systems localizes to both the plasma membrane and Golgi and integrates membrane trafficking with the dynamic localization of polarity proteins.[94] The mechanisms underlying linkage in *Tetrahymena* between the Golgi and cortical architecture remain to be explored. One avenue may be further analysis of *CDA12*, encoding a ciliate-restricted protein whose localization resembles Rab6Cp and Gef1p, and which is required for proper cell division.[31] The results in this paper suggest that in ciliates the organization of the secretory pathway could provide important determinants for both local and global patterning.

Limitations of the study

This study in *Tetrahymena* depends upon tracing the trajectory of a fluorescent heterologous protein that appears to undergo unregulated constitutive secretion from the cell. However, if the protein contains motifs that function as sorting signals in this system, or lacks important motifs present in endogenous secretory proteins, it may not fully represent all aspects of the constitutive secretory pathway in this organism. Our conclusions are based in part on using a basal body protein as a proxy for the parasomal sacs, which are known from numerous microscopic analyses to be adjacent to basal bodies. Due to technical obstacles related to limited detection of some fluorescent proteins, we were not able to show more directly that protein secretion occurs precisely at parasomal sacs. Similarly, our conclusions regarding sites of protein secretion are limited by the potential inability to visualize low levels of the fluorescent secretory protein, so we therefore cannot rule out minor levels of secretion at sites not detected in our study. Our study relies on some compartmental markers, e.g., Rab6 paralogs for the Golgi, whose inferred compartmental specificity is based on the published literature describing homologs in other lineages. The rigorous characterization of such markers in *Tetrahymena* or other ciliates would increase the confidence of our assignments.

RESOURCE AVAILABILITY

Lead contact

Further information and requests for resources and reagents should be directed to and will be fulfilled by the lead contact, Aaron P. Turkewitz (apturkew@uchicago.edu).

Materials availability

Strains used and plasmids generated in this study are available from the lead contact upon request.

Data and code availability

- Original western blot images, DOI, microscopy data and any additional information reported are available from the lead contact upon request.
- This paper does not report original code.

- Any additional information required to reanalyze the data reported in this paper is available from the lead contact upon request.

ACKNOWLEDGMENTS

S.K.'s laboratory is funded by Department of Biotechnology (DBT), Ministry of Science and Technology India (Ref no: BT/PR38584/MED/122/247/202), Department of Science and Technology (DST), Ministry Of Science And Technology India (Ref no: CRG/2021/000732) and DBT/Wellcome Trust India Alliance (Ref no: IA/I/22/2/506480).

A.P.T. was supported by the National Institutes of Health (NIH) (GM105783) and the National Science Foundation (MCB 1937326).

Y-.Y.J. and A.P.T. gratefully acknowledge help from Ed Munro and members of his laboratory (Universitay of Chicago) for help with TIRF microscopy, Chad Pearson, and Alex Stemm-Wolf (Univ of Colorado Anschutz Medical Campus, Aurora, CO) for providing the Poc1 construct, and Chao-Yin Cheng (University of Chicago) for many helpful discussions.

AUTHOR CONTRIBUTIONS

Conceptualization, Y-.Y.J. and A.P.T.; methodology, Y-.Y.J.; formal analysis, Y-.Y.J.; investigation, Y-.Y.J. and S.K.; resources, S.K. and A.P.T.; writing—original draft, Y-.Y.J. and A.P.T.; writing—review and editing, Y-.Y.J. and A.P.T.; visualization, Y-.Y.J.; supervision, A.P.T.; funding acquisition, S.K. and A.P.T.

DECLARATION OF INTERESTS

The authors declare no competing interests.

STAR★METHODS

Detailed methods are provided in the online version of this paper and include the following:

- KEY RESOURCES TABLE
- EXPERIMENTAL MODEL AND STUDY PARTICIPANT DETAILS
  - Growth of Tetrahymena thermophila cells
  - Strains used in this study
- METHOD DETAILS
  - Plasmid construction
  - Transformation and culture
  - Live-imaging and TIRF microscopy
  - ESCargo secretion assay and western blotting
- QUANTIFICATION AND STATISTICAL ANALYSIS
  - Quantification of western blotting
  - Measuring colocalization using Pearson coefficient

SUPPLEMENTAL INFORMATION

Supplemental information can be found online at https://doi.org/10.1016/j.isci.2024.111123.

Received: July 17, 2024
Revised: August 19, 2024
Accepted: October 4, 2024
Published: October 9, 2024

REFERENCES

1. Uhlén, M., Karlsson, M.J., Hober, A., Svensson, A.-S., Scheffel, J., Kotol, D., Zhong, W., Tebani, A., Strandberg, L., Edfors, F., et al. (2019). The human secretome. Sci. Signal. *12*, eaaz0274. https://doi.org/10.1126/scisignal.aaz0274.
2. Bonifacino, J.S., and Glick, B.S. (2004). The Mechanisms of Vesicle Budding and Fusion. Cell *116*, 153–166. https://doi.org/10.1016/S0092-8674(03)01079-1.
3. Raote, I., Saxena, S., and Malhotra, V. (2023). Sorting and Export of Proteins at the Endoplasmic Reticulum. Cold Spring Harb. Perspect. Biol. *15*, a041258. https://doi.org/10.1101/cshperspect.a041258.
4. Südhof, T.C., and Rothman, J.E. (2009). Membrane Fusion: Grappling with SNARE and SM Proteins. Science *323*, 474–477. https://doi.org/10.1126/science.1161748.
5. Jahn, R., Cafiso, D.C., and Tamm, L.K. (2024). Mechanisms of SNARE proteins in membrane fusion. Nat. Rev. Mol. Cell Biol. *25*, 101–118. https://doi.org/10.1038/s41580-023-00668-x.
6. Burgoyne, R.D., and Morgan, A. (2003). Secretory Granule Exocytosis. Physiol. Rev. *83*, 581–632. https://doi.org/10.1152/physrev.00031.2002.
7. Burgess, T.L., and Kelly, R.B. (1987). Constitutive and Regulated Secretion of Proteins. Annu. Rev. Cell Biol. *3*, 243–293. https://doi.org/10.1146/annurev.cb.03.110187.001331.
8. Li, R., Zhao, R., Yang, M., Zhang, X., and Lin, J. (2023). Membrane microdomains: Structural and signaling platforms for establishing membrane polarity. Plant Physiol. *193*, 2260–2277. https://doi.org/10.1093/plphys/kiad444.
9. Polgar, N., and Fogelgren, B. (2018). Regulation of Cell Polarity by Exocyst-Mediated Trafficking. Cold Spring Harb. Perspect. Biol. *10*, a031401. https://doi.org/10.1101/cshperspect.a031401.
10. Corliss, J.O. (2016). The Ciliated Protozoa: Characterization, Classification and Guide to the Literature (Elsevier).
11. Adl, S.M., Simpson, A.G.B., Lane, C.E., Lukeš, J., Bass, D., Bowser, S.S., Brown, M.W., Burki, F., Dunthorn, M., Hampl, V., et al. (2012). The Revised Classification of Eukaryotes. J. Eukaryot. Microbiol. *59*, 429–493. https://doi.org/10.1111/j.1550-7408.2012.00644.x.
12. Stelly, N., Halpern, S., Nicolas, G., Fragu, P., and Adoutte, A. (1995). Direct visualization of a vast cortical calcium compartment in Paramecium by secondary ion mass spectrometry (SIMS) microscopy: possible involvement in exocytosis. J. Cell Sci. *108*, 1895–1909. https://doi.org/10.1242/jcs.108.5.1895.
13. Allen, R.D. (1967). Fine Structure, Reconstruction and Possible Functions of Components of the Cortex of Tetrahymena pyriformis. J. Protozool. *14*, 553–565.

https://doi.org/10.1111/j.1550-7408.1967.tb02042.x.
14. Koreny, L., Mercado-Saavedra, B.N., Klinger, C.M., Barylyuk, K., Butterworth, S., Hirst, J., Rivera-Cuevas, Y., Zaccai, N.R., Holzer, V.J.C., Klingl, A., et al. (2023). Stable endocytic structures navigate the complex pellicle of apicomplexan parasites. Nat. Commun. *14*, 2167. https://doi.org/10.1038/s41467-023-37431-x.
15. Satir, B.H., and Wissig, S.L. (1982). Alveolar sacs of Tetrahymena: ultrastructural characteristics and similarities to subsurface cisterns of muscle and nerve. J. Cell Sci. *55*, 13–33. https://doi.org/10.1242/jcs.55.1.13.
16. Alimenti, C., Buonanno, F., Di Giuseppe, G., Guella, G., Luporini, P., Ortenzi, C., and Vallesi, A. (2022). Bioactive molecules from ciliates: Structure, activity, and applicative potential. J. Eukaryot. Microbiol. *69*, e12887. https://doi.org/10.1111/jeu.12887.
17. Bowman, G.R., Elde, N.C., Morgan, G., Winey, M., and Turkewitz, A.P. (2005). Core formation and the acquisition of fusion competence are linked during secretory granule maturation in Tetrahymena. Traffic (Copenhagen, Denmark) *6*, 303–323. https://doi.org/10.1111/j.1600-0854.2005.00273.x.
18. Luporini, P., Vallesi, A., Miceli, C., and Bradshaw, R.A. (1995). Chemical Signaling in Ciliates. J. Eukaryot. Microbiol. *42*, 208–212. https://doi.org/10.1111/j.1550-7408.1995.tb01567.x.
19. Plattner, H. (2017). Trichocysts—Paramecium's Projectile-like Secretory Organelles. J. Eukaryot. Microbiol. *64*, 106–133. https://doi.org/10.1111/jeu.12332.
20. Satir, B., Schooley, C., and Satir, P. (1973). MEMBRANE FUSION IN A MODEL SYSTEM : Mucocyst Secretion in Tetrahymena. J. Cell Biol. *56*, 153–176. https://doi.org/10.1083/jcb.56.1.153.
21. Vayssié, L., Skouri, F., Sperling, L., and Cohen, J. (2000). Molecular genetics of regulated secretion in Paramecium. Biochimie *82*, 269–288. https://doi.org/10.1016/S0300-9084(00)00201-7.
22. Turkewitz, A.P. (2004). Out with a Bang! Tetrahymena as a Model System to Study Secretory Granule Biogenesis. Traffic *5*, 63–68. https://doi.org/10.1046/j.1600-0854.2003.00155.x.
23. Cova, M.M., Lamarque, M.H., and Lebrun, M. (2022). How Apicomplexa Parasites Secrete and Build Their Invasion Machinery. Annu. Rev. Microbiol. *76*, 619–640. https://doi.org/10.1146/annurev-micro-041320-021425.
24. Satir, B.H., and Oberg, S.G. (1978). Paramecium Fusion Rosettes: Possible Function as Ca2+ Gates. Science *199*, 536–538. https://doi.org/10.1126/science.341312.
25. Sparvoli, D., and Lebrun, M. (2021). Unraveling the Elusive Rhoptry Exocytic Mechanism of Apicomplexa. Trends Parasitol. *37*, 622–637. https://doi.org/10.1016/j.pt.2021.04.011.
26. Madinger, C.L., Collins, K., Fields, L.G., Taron, C.H., and Benner, J.S. (2010). Constitutive Secretion in Tetrahymena thermophila. Eukaryot. Cell *9*, 674–681. https://doi.org/10.1128/EC.00024-10.
27. Casler, J.C., Zajac, A.L., Valbuena, F.M., Sparvoli, D., Jeyifous, O., Turkewitz, A.P., Horne-Badovinac, S., Green, W.N., and Glick, B.S. (2020). ESCargo: a regulatable fluorescent secretory cargo for diverse model organisms. Mol. Biol. Cell *31*, 2892–2903. https://doi.org/10.1091/mbc.E20-09-0591.
28. Franke, W.W., Eckert, W.A., and Krien, S. (1971). Cytomembrane differentiation in a ciliate, Tetrahymena pyriformis. Z.Zellforsch *119*, 577–604. https://doi.org/10.1007/BF00455249.
29. Pillai, A.N., Shukla, S., and Rahaman, A. (2017). An evolutionarily conserved phosphatidate phosphatase maintains lipid droplet number and endoplasmic reticulum morphology but not nuclear morphology. Biol. Open *6*, 1629–1643. https://doi.org/10.1242/bio.028233.
30. Kurz, S., and Tiedtke, A. (1993). The Golgi Apparatus of Tetrahymena Thermophila. J. Eukaryot. Microbiol. *40*, 10–13. https://doi.org/10.1111/j.1550-7408.1993.tb04874.x.
31. Zweifel, E., Smith, J., Romero, D., Giddings, T.H., Winey, M., Honts, J., Dahlseid, J., Schneider, B., and Cole, E.S. (2009). Nested Genes CDA12 and CDA13 Encode Proteins Associated with Membrane Trafficking in the Ciliate Tetrahymena thermophila. Eukaryot. Cell *8*, 899–912. https://doi.org/10.1128/ec.00342-08.
32. Bright, L.J., Kambesis, N., Nelson, S.B., Jeong, B., and Turkewitz, A.P. (2010). Comprehensive analysis reveals dynamic and evolutionary plasticity of Rab GTPases and membrane traffic in Tetrahymena thermophila. PLoS Genet. *6*, e1001155. https://doi.org/10.1371/journal.pgen.1001155.
33. Frankel, J. (2000). Cell biology of Tetrahymena thermophila. Methods Cell Biol. *62*, 27–125. https://doi.org/10.1016/s0091-679x(08)61528-9.
34. Aufderheide, K. (1979). Mitochondrial associations with specific microtubular components of the cortex of Tetrahymena thermophila. I. Cortical patterning of mitochondria. J. Cell Sci. *39*, 299–312. https://doi.org/10.1242/jcs.39.1.299.
35. Wloga, D., and Frankel, J. (2012). From Molecules to Morphology: Cellular Organization of *Tetrahymena thermophila*. In Methods in Cell Biology Tetrahymena Thermophila, K. Collins, ed. (Academic Press), pp. 83–140. https://doi.org/10.1016/B978-0-12-385967-9.00005-0.
36. PITELKA, D.R. (1961). Fine Structure of the Silverline and Fibrillar Systems of Three Tetrahymenid Ciliates. J. Protozool. *8*, 75–89. https://doi.org/10.1111/j.1550-7408.1961.tb01186.x.
37. Williams, N.E., and Luft, J.H. (1968). Use of a nitrogen mustard derivative in fixation for electron microscopy and observations on the ultrastructure of *Tetrahymena*. J. Ultrastruct. Res. *25*, 271–292. https://doi.org/10.1016/S0022-5320(68)80074-7.
38. Benmerah, A. (2013). The ciliary pocket. Curr. Opin. Cell Biol. *25*, 78–84. https://doi.org/10.1016/j.ceb.2012.10.011.
39. Clement, C.A., Ajbro, K.D., Koefoed, K., Vestergaard, M.L., Veland, I.R., Henriques de Jesus, M.P.R., Pedersen, L.B., Benmerah, A., Andersen, C.Y., Larsen, L.A., and Christensen, S.T. (2013). TGF-β signaling is associated with endocytosis at the pocket region of the primary cilium. Cell Rep. *3*, 1806–1814. https://doi.org/10.1016/j.celrep.2013.05.020.
40. Field, M.C., and Carrington, M. (2009). The trypanosome flagellar pocket. Nat. Rev. Microbiol. *7*, 775–786. https://doi.org/10.1038/nrmicro2221.
41. Molla-Herman, A., Ghossoub, R., Blisnick, T., Meunier, A., Serres, C., Silbermann, F., Emmerson, C., Romeo, K., Bourdoncle, P., Schmitt, A., et al. (2010). The ciliary pocket: an endocytic membrane domain at the base of primary and motile cilia. J. Cell Sci. *123*, 1785–1795. https://doi.org/10.1242/jcs.059519.
42. Allen, R.D., Schroeder, C.C., and Fok, A.K. (1992). Endosomal system of Paramecium: coated pits to early endosomes. J. Cell Sci. *101*, 449–461. https://doi.org/10.1242/jcs.101.2.449.
43. Elde, N.C., Morgan, G., Winey, M., Sperling, L., and Turkewitz, A.P. (2005). Elucidation of clathrin-mediated endocytosis in tetrahymena reveals an evolutionarily convergent recruitment of dynamin. PLoS Genet. *1*, e52. https://doi.org/10.1371/journal.pgen.0010052.
44. Nilsson, J.R., and van Deurs, B. (1983). Coated pits with pinocytosis in Tetrahymena. J. Cell Sci. *63*, 209–222. https://doi.org/10.1242/jcs.63.1.209.
45. Flötenmeyer, M., Momayezi, M., and Plattner, H. (1999). Immunolabeling analysis of biosynthetic and degradative pathways of cell surface components (glycocalyx) in *Paramecium cells*. Eur. J. Cell Biol. *78*, 67–77. https://doi.org/10.1016/S0171-9335(99)80008-9.
46. Fish, K.N. (2022). Total Internal Reflection Fluorescence (TIRF) Microscopy. Curr. Protoc. *2*, e517. https://doi.org/10.1002/cpz1.517.
47. Jiang, Y.Y., Lechtreck, K., and Gaertig, J. (2015). Total internal reflection fluorescence microscopy of intraflagellar transport in Tetrahymena thermophila. Methods Cell Biol. *127*, 445–456. https://doi.org/10.1016/bs.mcb.2015.01.001.
48. Shang, Y., Li, B., and Gorovsky, M.A. (2002). Tetrahymena thermophila contains a conventional γ-tubulin that is differentially required for the maintenance of different microtubule-organizing centers. J. Cell Biol. *158*, 1195–1206. https://doi.org/10.1083/jcb.200205101.
49. Barrero, J.J., Papanikou, E., Casler, J.C., Day, K.J., and Glick, B.S. (2016). An improved reversibly dimerizing mutant of the FK506-binding protein FKBP. Cell. Logist. *6*, e1204848. https://doi.org/10.1080/21592799.2016.1204848.
50. Casler, J.C., Papanikou, E., Barrero, J.J., and Glick, B.S. (2019). Maturation-driven transport and AP-1–dependent recycling of a secretory cargo in the Golgi. J. Cell Biol. *218*, 1582–1601. https://doi.org/10.1083/jcb.201807195.
51. Cowan, A.T., Bowman, G.R., Edwards, K.F., Emerson, J.J., and Turkewitz, A.P. (2005). Genetic, genomic, and functional analysis of the granule lattice proteins in Tetrahymena secretory granules. Mol. Biol. Cell *16*, 4046–4060. https://doi.org/10.1091/mbc.e05-01-0028.
52. Cheng, C.-Y., Romero, D.P., Zoltner, M., Yao, M.-C., and Turkewitz, A.P. (2023). Structure and dynamics of the contractile vacuole complex in Tetrahymena thermophila. J. Cell Sci. *136*, jcs261511. https://doi.org/10.1242/jcs.261511.
53. Pearson, C.G., Osborn, D.P.S., Giddings, T.H., Jr., Beales, P.L., and Winey, M. (2009). Basal body stability and ciliogenesis requires the conserved component Poc1.

J. Cell Biol. *187*, 905–920. https://doi.org/10.1083/jcb.200908019.
54. Hanada, K. (2024). Metabolic channeling of lipids via the contact zones between different organelles. Bioessays *46*, e2400045. https://doi.org/10.1002/bies.202400045.
55. AhYoung, A.P., Jiang, J., Zhang, J., Khoi Dang, X., Loo, J.A., Zhou, Z.H., and Egea, P.F. (2015). Conserved SMP domains of the ERMES complex bind phospholipids and mediate tether assembly. Proc. Natl. Acad. Sci. USA *112*, E3179–E3188. https://doi.org/10.1073/pnas.1422363112.
56. Kawano, S., Tamura, Y., Kojima, R., Bala, S., Asai, E., Michel, A.H., Kornmann, B., Riezman, I., Riezman, H., Sakae, Y., et al. (2018). Structure–function insights into direct lipid transfer between membranes by Mmm1–Mdm12 of ERMES. J. Cell Biol. *217*, 959–974. https://doi.org/10.1083/jcb.201704119.
57. Weide, T., Herrmann, L., Bockau, U., Niebur, N., Aldag, I., Laroy, W., Contreras, R., Tiedtke, A., and Hartmann, M.W.W. (2006). Secretion of functional human enzymes by Tetrahymena thermophila. BMC Biotechnol. *6*, 19. https://doi.org/10.1186/1472-6750-6-19.
58. Casanova, J.E. (2007). Regulation of Arf Activation: the Sec7 Family of Guanine Nucleotide Exchange Factors. Traffic *8*, 1476–1485. https://doi.org/10.1111/j.1600-0854.2007.00634.x.
59. Donaldson, J.G., and Jackson, C.L. (2011). ARF family G proteins and their regulators: roles in membrane transport, development and disease. Nat. Rev. Mol. Cell Biol. *12*, 362–375. https://doi.org/10.1038/nrm3117.
60. Shaner, N.C., Lambert, G.G., Chammas, A., Ni, Y., Cranfill, P.J., Baird, M.A., Sell, B.R., Allen, J.R., Day, R.N., Israelsson, M., et al. (2013). A bright monomeric green fluorescent protein derived from Branchiostoma lanceolatum. Nat. Methods *10*, 407–409. https://doi.org/10.1038/nmeth.2413.
61. Niyogi, S., Mucci, J., Campetella, O., and Docampo, R. (2014). Rab11 Regulates Trafficking of Trans-sialidase to the Plasma Membrane through the Contractile Vacuole Complex of Trypanosoma cruzi. PLoS Pathog. *10*, e1004224. https://doi.org/10.1371/journal.ppat.1004224.
62. Palade, G. (1975). Intracellular Aspects of the Process of Protein Synthesis. Science *189*, 347–358. https://doi.org/10.1126/science.1096303.
63. Rothblatt, J., and Schekman, R. (1989). Chapter 1 A Hitchhiker's Guide to Analysis of the Secretory Pathway in Yeast. In Methods in Cell Biology Vesicular Transport Part B, A.M. Tartakoff, ed. (Academic Press), pp. 3–36. https://doi.org/10.1016/S0091-679X(08)61165-6.
64. Lynch, M., Field, M.C., Goodson, H.V., Malik, H.S., Pereira-Leal, J.B., Roos, D.S., Turkewitz, A.P., and Sazer, S. (2014). Evolutionary cell biology: Two origins, one objective. Proc. Natl. Acad. Sci. USA *111*, 16990–16994. https://doi.org/10.1073/pnas.1415861111.
65. De la Concepcion, J.C. (2023). The exocyst complex is an evolutionary battleground in plant-microbe interactions. Curr. Opin. Plant Biol. *76*, 102482. https://doi.org/10.1016/j.pbi.2023.102482.
66. Ren, Y., Wang, Y., Zhang, Y., Pan, T., Duan, E., Bao, X., Zhu, J., Teng, X., Zhang, P., Gu, C., et al. (2022). Endomembrane-mediated storage protein trafficking in plants: Golgi-dependent or Golgi-independent? FEBS Lett. *596*, 2215–2230. https://doi.org/10.1002/1873-3468.14374.
67. Rui, Q., Tan, X., Liu, F., and Bao, Y. (2022). An Update on the Key Factors Required for Plant Golgi Structure Maintenance. Front. Plant Sci. *13*, 933283. https://doi.org/10.3389/fpls.2022.933283.
68. Ben Chaabene, R., Lentini, G., and Soldati-Favre, D. (2021). Biogenesis and discharge of the rhoptries: Key organelles for entry and hijack of host cells by the Apicomplexa. Mol. Microbiol. *115*, 453–465. https://doi.org/10.1111/mmi.14674.
69. Briguglio, J.S., Kumar, S., and Turkewitz, A.P. (2013). Lysosomal sorting receptors are essential for secretory granule biogenesis in Tetrahymena. J. Cell Biol. *203*, 537–550. https://doi.org/10.1083/jcb.201305086.
70. Ngô, H.M., Yang, M., and Joiner, K.A. (2004). Are rhoptries in Apicomplexan parasites secretory granules or secretory lysosomal granules? Mol. Microbiol. *52*, 1531–1541. https://doi.org/10.1111/j.1365-2958.2004.04056.x.
71. Bowman, G.R., and Turkewitz, A.P. (2001). Analysis of a Mutant Exhibiting Conditional Sorting to Dense Core Secretory Granules in Tetrahymena thermophila. Genetics *159*, 1605–1616. https://doi.org/10.1093/genetics/159.4.1605.
72. Chilcoat, N.D., Melia, S.M., Haddad, A., and Turkewitz, A.P. (1996). Granule lattice protein 1 (Grl1p), an acidic, calcium-binding protein in Tetrahymena thermophila dense-core secretory granules, influences granule size, shape, content organization, and release but not protein sorting or condensation. J. Cell Biol. *135*, 1775–1787. https://doi.org/10.1083/jcb.135.6.1775.
73. Barlowe, C., and Helenius, A. (2016). Cargo Capture and Bulk Flow in the Early Secretory Pathway. Annu. Rev. Cell Dev. Biol. *32*, 197–222. https://doi.org/10.1146/annurev-cellbio-111315-125016.
74. Cole, E.S., Maier, W., Joachimiak, E., Jiang, Y.Y., Lee, C., Collet, E., Chmelik, C., Romero, D.P., Chalker, D., Alli, N.K., et al. (2023). The Tetrahymena bcd1 mutant implicates endosome trafficking in ciliate, cortical pattern formation. MBoC *34*, ar82. https://doi.org/10.1091/mbc.E22-11-0501.
75. Jiang, Y.Y., Maier, W., Baumeister, R., Joachimiak, E., Ruan, Z., Kannan, N., Clarke, D., Louka, P., Guha, M., Frankel, J., and Gaertig, J. (2019). Two Antagonistic Hippo Signaling Circuits Set the Division Plane at the Medial Position in the Ciliate Tetrahymena. Genetics *211*, 651–663. https://doi.org/10.1534/genetics.118.301889.
76. Jiang, Y.Y., Maier, W., Chukka, U.N., Choromanski, M., Lee, C., Joachimiak, E., Wloga, D., Yeung, W., Kannan, N., Frankel, J., and Gaertig, J. (2020). Mutual antagonism between Hippo signaling and cyclin E drives intracellular pattern formation. J. Cell Biol. *219*, e202002077. https://doi.org/10.1083/jcb.202002077.
77. Jiang, Y.Y., Maier, W., Baumeister, R., Minevich, G., Joachimiak, E., Ruan, Z., Kannan, N., Clarke, D., Frankel, J., and Gaertig, J. (2017). The Hippo Pathway Maintains the Equatorial Division Plane in the Ciliate Tetrahymena. Genetics *206*, 873–888. https://doi.org/10.1534/genetics.117.200766.
78. Lee, C., Maier, W., Jiang, Y.-Y., Nakano, K., Lechtreck, K.F., and Gaertig, J. (2024). Global and local functions of the Fused kinase ortholog CdaH in intracellular patterning in Tetrahymena. J. Cell Sci. *137*, jcs261256. https://doi.org/10.1242/jcs.261256.
79. Tavares, A., Gonçalves, J., Florindo, C., Tavares, A.A., and Soares, H. (2012). Mob1: defining cell polarity for proper cell division. J. Cell Sci. *125*, 516–527. https://doi.org/10.1242/jcs.096610.
80. Cole, E., and Gaertig, J. (2022). Anterior-posterior pattern formation in ciliates. J. Eukaryot. Microbiol. *69*, e12890. https://doi.org/10.1111/jeu.12890.
81. Maritzen, T., and Haucke, V. (2018). Coupling of exocytosis and endocytosis at the presynaptic active zone. Neurosci. Res. *127*, 45–52. https://doi.org/10.1016/j.neures.2017.09.013.
82. Zhang, L., Xing, J., and Lin, J. (2019). At the intersection of exocytosis and endocytosis in plants. New Phytol. *224*, 1479–1489. https://doi.org/10.1111/nph.16018.
83. Guerrier, S., Plattner, H., Richardson, E., Dacks, J.B., and Turkewitz, A.P. (2017). An evolutionary balance: conservation vs innovation in ciliate membrane trafficking. Traffic *18*, 18–28. https://doi.org/10.1111/tra.12450.
84. Allen, R.D., and Fok, A.K. (1980). Membrane recycling and endocytosis in Paramecium confirmed by horseradish peroxidase pulse-chase studies. J. Cell Sci. *45*, 131–145. https://doi.org/10.1242/jcs.45.1.131.
85. McGinness, A.J., Schoberer, J., Pain, C., Brandizzi, F., and Kriechbaumer, V. (2022). On the nature of the plant ER exit sites. Front. Plant Sci. *13*, 1010569. https://doi.org/10.3389/fpls.2022.1010569.
86. Nebenführ, A., and Staehelin, L.A. (2001). Mobile factories: Golgi dynamics in plant cells. Trends Plant Sci. *6*, 160–167. https://doi.org/10.1016/s1360-1385(01)01891-x.
87. Takagi, J., Kimori, Y., Shimada, T., and Hara-Nishimura, I. (2020). Dynamic Capture and Release of Endoplasmic Reticulum Exit Sites by Golgi Stacks in Arabidopsis. iScience *23*, 101265. https://doi.org/10.1016/j.isci.2020.101265.
88. Al Jewari, C., and Baldauf, S.L. (2023). An excavate root for the eukaryote tree of life. Sci. Adv. *9*, eade4973. https://doi.org/10.1126/sciadv.ade4973.
89. Gabaldón, T. (2021). Origin and Early Evolution of the Eukaryotic Cell. Annu. Rev. Microbiol. *75*, 631–647. https://doi.org/10.1146/annurev-micro-090817-062213.
90. Albisetti, A., Florimond, C., Landrein, N., Vidilaseris, K., Eggenspieler, M., Lesigang, J., Dong, G., Robinson, D.R., and Bonhivers, M. (2017). Interaction between the flagellar pocket collar and the hook complex via a novel microtubule-binding protein in Trypanosoma brucei. PLoS Pathog. *13*, e1006710. https://doi.org/10.1371/journal.ppat.1006710.
91. Kalb, L.C., Frederico, Y.C.A., Boehm, C., Moreira, C.M.d.N., Soares, M.J., and Field, M.C. (2016). Conservation and divergence within the clathrin interactome of

Trypanosoma cruzi. Sci. Rep. *6*, 31212. https://doi.org/10.1038/srep31212.

92. Bell, A.J., Guerra, C., Phung, V., Nair, S., Seetharam, R., and Satir, P. (2009). GEF1 is a ciliary Sec7 GEF of Tetrahymena thermophila. Cell Motil Cytoskeleton *66*, 483–499. https://doi.org/10.1002/cm.20348.
93. Kaczanowska, J., Joachimiak, E., Buzanska, L., Krawczynska, W., Wheatley, D.N., and Kaczanowski, A. (1999). Molecular Subdivision of the Cortex of Dividing *Tetrahymena* Is Coupled with the Formation of the Fission Zone. Dev. Biol. *212*, 150–164. https://doi.org/10.1006/dbio.1999.9362.
94. Ravichandran, Y., Goud, B., and Manneville, J.-B. (2020). The Golgi apparatus and cell polarity: Roles of the cytoskeleton, the Golgi matrix, and Golgi membranes. Curr. Opin. Cell Biol. *62*, 104–113. https://doi.org/10.1016/j.ceb.2019.10.003.
95. Busch, C.J.-L., Vogt, A., and Mochizuki, K. (2010). Establishment of a Cre/loxP recombination system for N-terminal epitope tagging of genes in Tetrahymena. BMC Microbiol. *10*, 191. https://doi.org/10.1186/1471-2180-10-191.
96. Cassidy-Hanley, D., Bowen, J., Lee, J.H., Cole, E., VerPlank, L.A., Gaertig, J., Gorovsky, M.A., and Bruns, P.J. (1997). Germline and Somatic Transformation of Mating Tetrahymena thermophila by Particle Bombardment. Genetics *146*, 135–147. https://doi.org/10.1093/genetics/146.1.135.
97. Sparvoli, D., Richardson, E., Osakada, H., Lan, X., Iwamoto, M., Bowman, G.R., Kontur, C., Bourland, W.A., Lynn, D.H., Pritchard, J.K., et al. (2018). Remodeling the Specificity of an Endosomal CORVET Tether Underlies Formation of Regulated Secretory Vesicles in the Ciliate Tetrahymena thermophila. Curr. Biol. *28*, 697–710.e13. https://doi.org/10.1016/j.cub.2018.01.047.
98. Kuppannan, A., Jiang, Y.-Y., Maier, W., Liu, C., Lang, C.F., Cheng, C.-Y., Field, M.C., Zhao, M., Zoltner, M., and Turkewitz, A.P. (2022). A novel membrane complex is required for docking and regulated exocytosis of lysosome-related organelles in Tetrahymena thermophila. PLoS Genet. *18*, e1010194. https://doi.org/10.1371/journal.pgen.1010194.
99. Robin, F.B., McFadden, W.M., Yao, B., and Munro, E.M. (2014). Single-molecule analysis of cell surface dynamics in Caenorhabditis elegans embryos. Nat. Methods *11*, 677–682. https://doi.org/10.1038/nmeth.2928.
100. Schindelin, J., Arganda-Carreras, I., Frise, E., Kaynig, V., Longair, M., Pietzsch, T., Preibisch, S., Rueden, C., Saalfeld, S., Schmid, B., et al. (2012). Fiji: an open-source platform for biological-image analysis. Nat. Methods *9*, 676–682. https://doi.org/10.1038/nmeth.2019.
101. Bolte, S., and Cordelières, F.P. (2006). A guided tour into subcellular colocalization analysis in light microscopy. J. Microsc. *224*, 213–232. https://doi.org/10.1111/j.1365-2818.2006.01706.x.

STAR★METHODS

KEY RESOURCES TABLE

REAGENT or RESOURCE	SOURCE	IDENTIFIER
Antibodies		
anti-FBKP	Abcam	Ab2918; RRID:AB_303413
Experimental models: Organisms/strains		
T. thermophila: ESCargo	This study	
T. thermophila: GFP-KDEL	This study	
T. thermophila: Poc1-GFP	This study	
T. thermophila: Poc1-mcherry	This study	
T. thermophila: GFP-Rab6C	This study	
T. thermophila: Gef1-GFP	This study	
T. thermophila: Gef1-mNeon	This study	
Recombinant DNA		
pNeo5_ESCargo	This study	
pNeo5_ESCargo_GFP-KDEL	This study	
pPur4_Poc1-GFP	This study	
pNeo4_Poc1-3mCherry	This study	
pPur4_mEGFP-Rab6C	This study	
pPur4_Gef1-mGFP	This study	
pkiGEF1-mNeon-neo4	This study	
Other		
MitoTracker Green FM	Invitrogen	M7514
Cygel	Abcam	Ab109204
SLF	Cayman	10007974

EXPERIMENTAL MODEL AND STUDY PARTICIPANT DETAILS

Growth of Tetrahymena thermophila cells

Tetrahymena thermophila cells were grown in SPP medium: 2% proteose peptone (Gibco, 211684), 0.1% yeast extract (BD 212750), 0.2% dextrose (ACROS 41095-5000) and 0.003% EDTA, ferric-sodium salt (Sigma). Prior to use, the medium (SPPA) was supplemented with 100 μg/mL Normocin (InvivoGen ant-nr-05). Cells were grown at 30°C in 15 mL conical tubes placed horizontally or in flasks with agitation at 100 rpm.

Strains used in this study

ESCargo, GFP-KDEL, Poc1-GFP, Poc1-mcherry, GFP-Rab6C, Gef1-GFP, Gef1-mNeon.

METHOD DETAILS

Plasmid construction

A construct comprised sequentially of the *MTT1* promoter, the 18 residue *GRL1* signal sequence, the ESCargo* coding sequence[27] and the *BTU1* 3′ flanking sequence was added to one side of a *neo5* paromomycin-resistance marker.[75,95] The *MTT1* 3′ flanking sequence was added to the other side of the *neo5* marker, so that ssGrl1-ESCargo-neo5 will integrate by recombination at the endogenous *MTT1* locus.

A construct comprised sequentially of the histone promoter (HHFI), a monomeric EGFP (mEGFP) coding sequence tailed by an AAG(K)-GAT(D)-GAA(E)-TTA(L) and the *BTU1* 3′ flanking sequence was added to the construct above following the *BTU1* 3′ sequence that flanks the ESCargo coding sequence. Recombination of the resulting construct will integrate both transgenes, ESCargo and ss-mEGFP-KDEL, into the *MTT1* locus.

The coding sequence of mEGFP was fused upstream to the coding sequence of *RAB6C* (*TTHERM_00079900*), which was followed by the *BTU1* 3′ flanking sequence and the pur4 selection marker.[32] This assembly was then flanked by the *Rab6C* 5′ and 3′ flanks, to direct the

integration of the whole construct at the endogenous *RAB6C* locus. For this gene we used N-terminal tagging, notwithstanding the possibility of perturbing transcriptional regulation, to avoid disrupting the predicted targeting signal at the C-terminus.

For endogenous tagging, the 1 kb fragments of the coding sequences ending at the stop codon (excluded) of *GEF1* (*TTHERM_00569500*), and *POC1* (*TTHERM_01308010*), and their respective 3′ flanking sequences, were used to add flanks to an in-frame mEGFP coding sequence followed by a *BTU1* 3′ flanking sequence and a *pur4* selection marker.[53,92] Separately, *POC1* was also natively tagged with mCherry using the same strategy, including flanking the mCherry2HA coding sequence with a *BTU1* flanking 3′ sequence and a *neo4* selection marker. To tag *GEF1*, a 0.7 kb fragment of the coding sequence ending with the stop codon (excluded) and a 0.7 kb 3′ fragment of *GEF1* were used to flank an in-frame 2xmNeon-6Myc coding sequence followed by a *BTU1* 3′ sequence and a *neo4* selection marker.

Transformation and culture

Plasmids were linearized to release the fragments for recombination. Biolistic transformations were performed with 900 psi rupture disks as previously described.[96,97] A notable change to the target cells carrier was to thinly spread the cell pellets from a 10–12 mL starved culture on a bed of Tris-Agar (10 mM Tris-HCl pH 7.4, 2% agar, Fisher BP1423) in 10 cm petri dishes. Following the biolistic bombardment, the target cells were resuspended in 10 mL SPPA media with appropriate drug(s) and distributed into a 96-well plates, 100 μL per well. For *neo5*-based transformation, the selection SPPA media contained 200 μg/mL paromomycin, gradually increased to 2000 μg/mL over 1–2 weeks. For *neo4*-based transformation, the selection SPPA media contained 1 μg/mL $CdCl_2$ and 100 μg/mL paromomycin, which was gradually switched to 0.01 μg/mL $CdCl_2$ and 800 μg/mL paromomycin over 1–2 weeks. For *pur4*-based transformation, the selection SPPA media initially contained 1 μg/mL $CdCl_2$ and 200 μg/mL puromycin and was gradually switched to 0.01 μg/mL $CdCl_2$ and 200 μg/mL puromycin over 1–2 weeks.

Live-imaging and TIRF microscopy

For live staining of mitochondria, MitoTracker Green FM (Invitrogen M7514) was added to a final concentration of 50 nM to the cell culture for 30 min followed by a brief wash with 10 mM Tris-HCl, pH 7.4.

Epifluorescent live-imaging was performed as previously described.[98] Briefly, an equal volume of cold Cygel (Abcam ab109204, buffered to 10 mM Tris-HCl, pH 7.4) was mixed 1:1 with cells washed with 10 mM Tris-HCl, pH 7.4, on prechilled coverslips placed on a cold dry surface (a heat block chilled in an ice bath). To observe dispersed ESCargo, cells with ESCargo aggregates were mixed into CyGel with added SLF (Cayman 10007974) up to 1 mM. In cases where precipitates were visible, the gel mixture was mixed gently prior to use.

Five-to-seven μL of sample was placed on a 22x22 coverslip. A room temperature glass slide was slowly lowered onto the CyGel/cell mixture and raised together with the coverslip. The assembled slide was placed for 20 s on a dry 37°C surface, followed by mounting to an Axiocam 702 mono using the Zeiss Axio Observer 7 system, with a 100X objective (Alpha Plan-Apo 100×/1.46 oil DIC M27).

TIRF microscopy was performed on an inverted Nikon Ti-E microscope as described in.[99] Total volume of CyGel-cell mixture was reduced to 3–5 μL in order to restrict cell movement and potentially limit the diffusion of secreted ESCargo.

ESCargo secretion assay and western blotting

ESCargo secretion was assayed by western blotting as previously described[27] with the following modifications. Cells incubated with $CdCl_2$ to induce ESCargo expression were washed and resuspended in 10 mM Tris-HCl, pH 7.4 prior to adding 12.5 μM SLF for the times indicated, followed by cell pelleting and trichloroacetic acid (TCA, 10%) precipitation of the cell-free supernatant. A rabbit monoclonal anti-FBKP antibody (Abcam ab2918) was diluted 1:2000 in 5% nonfat dry milk in TBST (50mM Tris-HCl, pH 7.5, 150 mM NaCl, 0.05% Tween 20) for overnight incubation with the blot.

QUANTIFICATION AND STATISTICAL ANALYSIS

Quantification of western blotting

Areas with the same dimension enclosing the perspective bands were selected and measured using Fiji.[100] The intensities were then standardized to the -SLF as 100%.

Measuring colocalization using Pearson coefficient

Images and videos are analyzed using Fiji.[100] Max intensity z-projection of select few continuous images from a time series were used to measure Pearson coefficients using JACoP plugin.[101]